Korean J. Chem. Eng., 37(3), 505-512 (2020)
DOI: 10.1007/s11814-019-0465-x

pISSN: 0256-1115
eISSN: 1975-7220

Carbon capture by alkaline absorbent using octadecyltrichlorosilane modified PVDF/TiO_2 membrane

Why-Ling Tan, Hoi-Fang Tan, Nor Aini Ahmad, Norhaziyana Hamzah, Abdul Latif Ahmad, and Choe Peng Leo†

School of Chemical Engineering, Engineering Campus, Universiti Sains Malaysia, 14300 Nibong Tebal, Pulau Pinang, Malaysia
(*Received 4 September 2019 • accepted 16 December 2019*)

Abstract−Carbon capture efficiency of membrane gas absorption was improved using a nearly superhydrophobic membrane. This membrane, polyvinylidene fluoride (PVDF) membrane, was blended with TiO_2 nanoparticles and post-modified with octadecyltrichloro silane to reduce wetting. Wetting reduction is important to minimize mass transfer resistance in membrane pores during carbon capture. The hydrophilic TiO_2 nanoparticles reduced membrane pore size and hydrophobicity in dual bath coagulation, but they offered active sites for silane modification as proven by Fourier-transform infrared spectra to achieve a water contact angle up to 148.8°. A non-wetting surface near to Cassie-Baxter state was formed due to the nano-roughness of TiO_2 nanoparticles and hydrophobic functional groups of silane. The modified membrane showed higher CO_2 absorption flux in comparison to the neat PVDF membrane, as much as 114% improvement. The modified membrane also achieved faster carbon capture into water. Furthermore, PVDF and PVDF/TiO_2 membranes modified with octadecyltrichloro silane in ethanol (volume ratio of 5 : 50) were less affected by NaOH absorbent, displaying great potential for carbon capture and storage using alkaline waste.

Keywords: Membrane, Absorption, PVDF, Alkaline

INTRODUCTION

Carbon dioxide (CO_2) emission from energy generation activities is one the major causes of global warming and climate change. Global CO_2 emissions reached 33.1 Gt gigatons in 2018, as reported by the International Energy Agency [1]. Several carbon capture and storage (CCS) projects commenced in the past few years after the success of the first commercial CCS project, Sleipner in Norway. Sleipner CCS project captured more than 1 million tons of CO_2 annually from natural gas using amine technology since 1996 [2]. More CCS projects have commenced in the past few years, including Petra Nova CCS facility in Texas, Emirates Steel CCS project at Abu Dhabi, Tomakomai CCS Demonstration Project in Japan and Illinois Industrial CCS project in Decatur [3-6].

In the past two decades, the researchers and technologists have also proposed more alternatives to elevate CCS mitigation strategies into carbon capture, utilization and storage (CCUS) initiatives at the same time. Mineral carbonation has been extensively studied because CO_2 can be sequestrated in the form of thermodynamically stable carbonates using different types of alkaline waste. The major routes of mineral carbonation are direct gas-solid carbonation, direct aqueous carbonation and indirect aqueous carbonation [7]. Direct gas-solid carbonation of fly ash has been widely reported, but the efficiency is lower than by aqueous carbonation. Direct aqueous carbonation, which involves dissolution and carbonation in the aqueous phase, can be further improved using different types of leaching agents such as acid and ammonium salts [8]. Part et al. and Kang et al. [9-11] focused on the indirect aqueous carbonation using carbon captured by alkanolamine absorbent which is conducted at low pressure and temperature before mixing with different types of calcium salts to form calcium carbonate which could be easily precipitated. More than 80% of calcium chloride and calcium hydroxide was converted into calcium carbonate using monoethanolamine in less than 100 min. On the other hand, seawater decalcification using CO_2 was studied [12]. The effects of temperature, salinities and pH on CO_2 dissolution into seawater were studied since the CO_2 dissolution rate was assumed to govern the precipitation rate of carbonates. The increment of seawater alkalinity accelerated the decalcification significantly. However, the decalcification rate decreased at pH 9.1 due to the competition between calcium and magnesium carbonation. Aragonite was precipitated with the pH range of 7.3-8.5, but monohydrocalcite and nesquehonite were also collected when the solution pH was increased to 9.1. Magnesium hydroxide was then proposed to replace NaOH in the decalcification reaction [13]. However, a reaction time of more than 150 min was required to achieve more than 90% decalcification using white clay from a soda ash production plant. Cheng et al. [14] further studied the formation of $MgCO_3$ from carbonation reaction using $Mg(OH)_2$. The formation of $MgCO_3$ could follow the dissolution-recrystallization mechanism. Hence, Dindi et al. [15] further proposed the production of carbonates using CO_2 and brine waste. Chlorides ions were removed from brine using hydrotalcite to form alkaline brine solution, which could be converted into $NaHCO_3$ via carbonation reaction. Zhang et al. [16] recently used nickel nanoparticle catalyst (30 ppm) to promote calcium carbonation efficiency about 10% by accelerating the rate-limiting step of carbonation reaction, namely, the carbonic acid formation in the alkaline solution.

†To whom correspondence should be addressed.
E-mail: chcpleo@usm.my

Table 1. The composition of membrane dope solution and silane modification

Membrane	PVDF (wt%)	NMP (wt%)	H_3PO_4 (wt%)	LiCl (wt%)	Acetone (wt%)	TiO_2 (wt%)	Volume ratio of silane to ethanol
P0	13	77	3	2	5	-	-
P0S	13	77	3	2	5	-	5 : 50
PT	13	74	3	2	5	3	-
PTS/2	13	74	3	2	5	3	1 : 50
PTS/10	13	74	3	2	5	3	5 : 50

As proposed by Ji et al. [8] and Salmón et al. [17], indirect aqueous carbonation could be integrated with carbon capture technology. Carbonates formed at 40 °C with the addition of CaO or fly ash into the CO_2 rich monoethanolamine as reported by Ji et al. [18]. Salmón et al. [17] concluded that CO_2 removal efficiency of NaOH in membrane contactor is higher than a packed column. Membranes are more compact than conventional columns, leading to a reduction over 70% in size and 66% in weight [19]. Although NaOH is useful in mineral carbonation without regeneration required, the stability of polymeric membrane in alkaline solution remains questionable. PVDF membrane degraded in NaOH and KOH solution with concentration as low as 0.01 M and the degradation was promoted by the elevated temperature [20]. Unlike alcohol amine absorbent, NaOH has not been extensively studied in membrane gas absorption research since lower CO_2 flux was reported [21]. This work's aim was to study the stability of PVDF membrane in membrane gas absorption using NaOH as the absorbent. The membrane was incorporated with inorganic filler, TiO_2 nanoparticles and modified with hydrophobic agent, octadecyltrichloro silane to create surface hydrophobicity for minimum contact with NaOH absorbent. Unlike our previous work [22] fluorohydrocarbon silanes were not used here due to their environmental impact. The CO_2 selectivity could be improved from 3.48 to 29.4 after embedding nanoparticles into PVDF membrane as reported in our previous work [23].

EXPERIMENTAL

1. Materials

PVDF (Solef® 6010, Solvay Solexis) and N-methyl-2-pyrrolidone (NMP) (>99.5%, Merck) were used to prepare the membrane dope solution. The membrane dope solution also contains orthophosphoric acid (H_3PO_4) (>85%, Merck), lithium chloride (LiCl, Merck) and acetone (Merck). TiO_2 nanoparticles (21 nm primary particle size, >99.5% trace metal basis) from Sigma-Aldrich and octadecyltrichloro silane from Gelest were used to enhance surface roughness and energy, respectively. Ethanol (>99.9%, Merck) was used in coagulation and silanation. NaOH (99%, Merck), HCl (37%, Merck) and phenolphthalein (>0.98%, Merck) were used in the titration of absorbent sample from membrane gas absorption.

2. Membrane Synthesis and Characterization

2-1. Membrane Synthesis

PVDF membrane was synthesized using dual bath coagulation as reported previously [24]. In brief, H_3PO_4 (3 wt%) was dissolved into NMP before adding the dried PVDF (15 wt%) to form the dope solution of PVDF membrane. TiO_2 nanoparticles (3 wt%) were first dispersed in NMP followed by non-solvent additives and polymer in the preparation of PVDF/TiO_2 membrane dope solution. All dope solution was stirred at 50 °C for one day and degassed for one day before casting. The dope solution was cast into thin film on woven support with a gap of 400 μm (Elcometer 4340 automatic). The film was immersed into ethanol for 20 min followed by distilled water for 24 h to form membrane. The dried membranes (40 °C for 72 h) were immersed into silane solution prepared at a volumetric ratio of 1 mL silane to 50 mL ethanol or 5 mL silane to 50 mL ethanol for 4 min. The modified membranes were rinsed with ethanol and dried at 40 °C for 24 h before characterization. Table 1 summarizes the dope and silane compositions for membranes prepared in this work.

2-2. Membrane Characterization

The morphology of membrane surface and cross-section were studied using scanning electron microscopy (SEM) (HITACHI S-3000N, Hitachi Ltd., Japan) with an acceleration voltage range of 0.3-30 kV. The membranes were cracked in liquid nitrogen before cross-sectional scanning.

The surface wetting was quantified in terms of water contact angle. Deionized (DI) water was dropped on the membrane surface using a syringe to form five water droplets at different positions for the replicated measurement by a goniometer (Ramé-Hart Instruments Co., USA). The mean water contact angle was determined from water contact angles measured at five different locations on the membrane surface.

Fourier transform infrared (FT-IR) spectroscopy (Nicolet iS10, Thermo Scientific, USA) was used to record the spectra from 600 cm^{-1} to 3,800 cm^{-1} for the understanding of chemical changes after silane modification.

3. Membrane Gas Absorption

The CO_2 absorption fluxes through the membranes were compared using a membrane gas absorption system described in our previous work [25,26]. The membrane module consists of a gas chamber and a liquid chamber separated by a membrane sample with an effective diameter of 3.9 cm. CO_2 gas (purity >99%) was fed into the membrane module at 100 mL/min while the distilled water was counter-currently fed into membrane module at 150 mL/min to initiate the comparison. The CO_2 concentration in four absorbent samples (50 ml) at outlet was determined using Eq. (2). A few drops of phenolphthalein were added into sample before titration using NaOH solution (0.01 M) until the appearance of pink color. Subsequently, the CO_2 absorption flux was determined using Eq. (2)

$$C_{CO_2}\left(\frac{\text{mol}}{\text{L}}\right)=\frac{M\cdot V_{NaOH}}{2V_{sample}} \quad (1)$$

$$CO_2\ \text{flux}=\frac{C_{CO_2}\times Q_{abs}}{A} \quad (2)$$

where M is NaOH concentration (mol/L), V_{NaOH} NaOH volume (L), V_{sample} is the absorbent sample volume (L), Q_{abs} is absorbent flow rate (L/s) and A is effective membrane surface area (m^2). NaOH was used as absorbent in the subsequent measurement of carbon storage potential. NaOH absorbent was recirculated back into membrane gas absorption system until depletion. In the presence of NaOH, carbonates were formed due to the absorption into NaOH solution. After NaOH depletion, bicarbonates could form. The overall reaction between CO_2 gas and NaOH solution can be stated as follows:

$$CO_2(g)+2NaOH(aq)\leftrightarrow Na_2CO_3(aq)+H_2O(l) \quad (3)$$

HCl was used in the titration of absorbent samples as described earlier to determine the NaOH and the total carbonate and bicarbonate concentration.

RESULTS AND DISCUSSION

1. Membrane Characteristics

The surface morphology of the P0, PT, P0S and PTS mem-

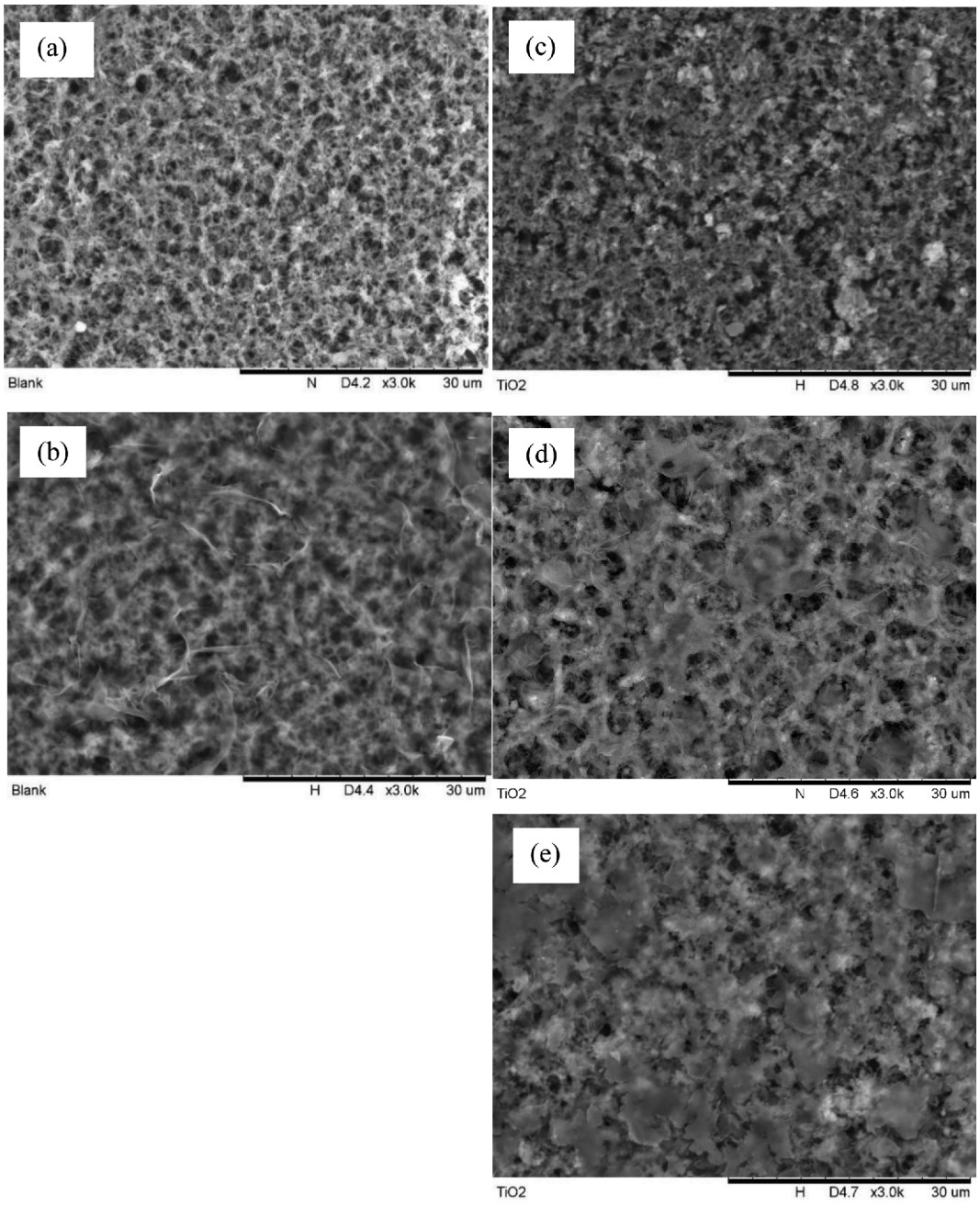

Fig. 1. SEM images of the surface of (a) P0 (b) P0S (c) PT, (d) PTS/2 and (e) PTS/10 membranes.

branes was studied using SEM images in Fig. 1. All the membranes exhibit spongy structure as reported in our previous work [22]. The non-solvent additive, LiCl encouraged the formation of large cavities and open structure [27]. LiCl interacts with NMP and PVDF to form LiCl-NMP and LiCl-PVDF complexes. The formation of these complexes caused the reduction of solvent strength (NMP) and dissolution of the polymer (PVDF), resulting in polymer aggregation for the formation of spongy structure [28]. Furthermore, PVDF membranes were fabricated using dual coagulation baths, ethanol followed by distilled water. Ethanol could delay the demixing process to promote the formation of porous structure with large pores and great roughness [26,27]. The porous structure of membrane was slightly affected once the TiO_2 was incorporated into PVDF membranes comparing Fig. 1(a) and (c). This is because the hydrophilic TiO_2 nanoparticles promote the penetration of non-solvent into the nascent membrane during phase inversion. Hydrophobic membranes with smaller pore size could achieve higher absorption rate because liquid penetrates less into the small pores, resulting in less hindrance to CO_2 transfer [29]. The mean pore size of P0 and PT membranes are 0.42 μm and 0.41 μm, respectively as stated in our previous work [22]. Silane modification caused more significant changes of surface morphology can be seen clearly by comparing between Fig. 1(a) to (b), and (c) to (d) or (e). The porous structure was hindered after silane modification. Octadec-

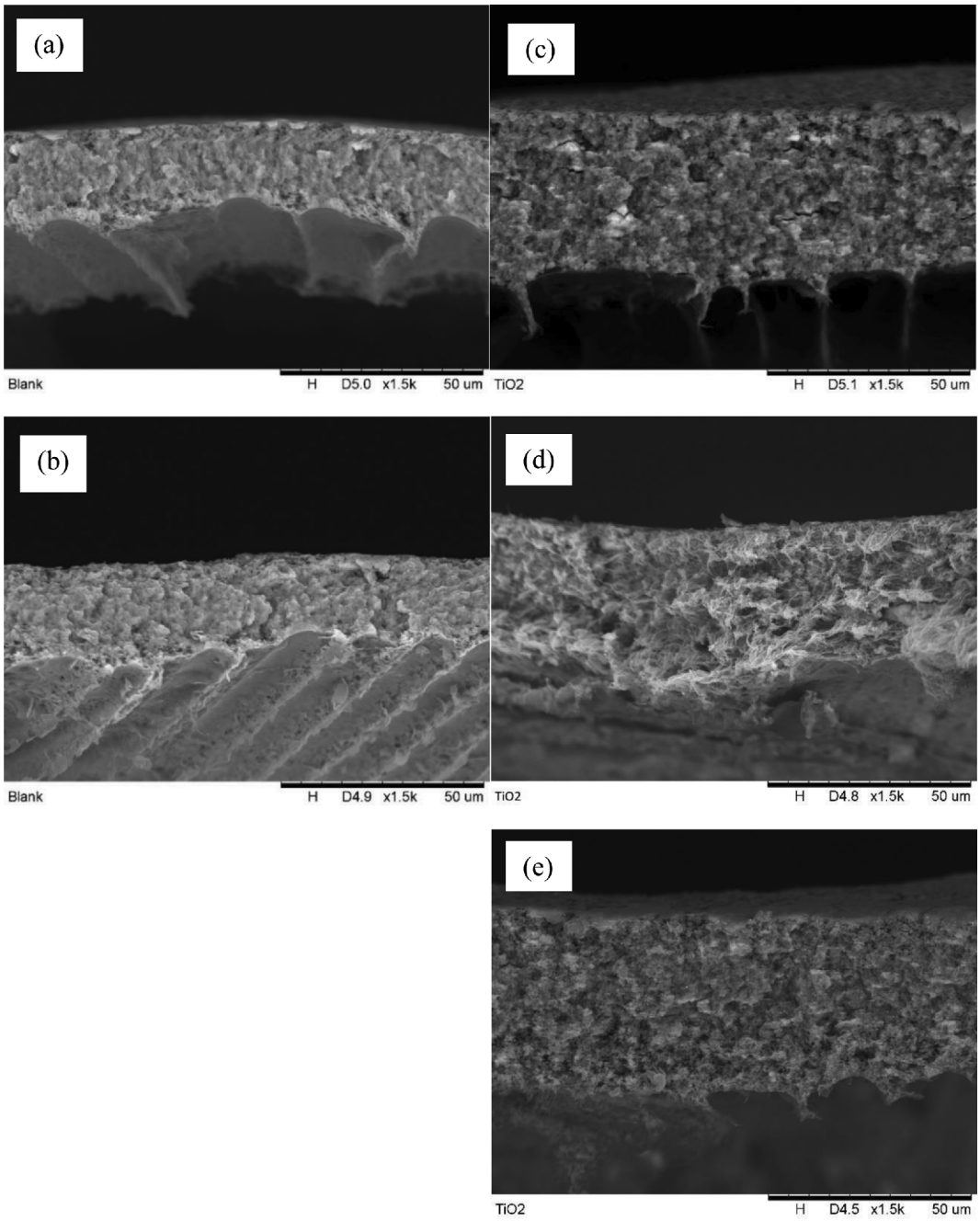

Fig. 2. SEM images of the cross-section of (a) P0 (b) P0S (c) PT, (d) PTS/2 and (e) PTS/10 membranes.

yltrichlorosilane is commonly used to form self-assembled monolayer via the hydrolysis of chlorosilane groups with water and the condensation of silanol groups with the surface hydroxyl groups [30]. However, the condensation of adjacent silanols could result in the formation of cross-linked mat as shown in the SEM images in Fig. 1(b), (d) and (e). The cross-section of P0, PT, P0S and PTS membranes was studied using SEM images presented in Fig. 2. The membrane thickness was increased by adding TiO_2 nanoparticles into PVDF dope solution. The increment could be observed by comparing PVDF/TiO_2 membranes (PT, PTS/2 and PTS/10) with the PVDF membranes (P0 and P0S) are as shown in Fig. 1(a) and (c). The increment of membrane thickness could be attributed by the increment of solution viscosity by nanoparticles reported by others [31]. The thickness of P0 membrane is 22.0 μm, while the thickness of PT membrane is 39.8 μm as measured from SEM images in Fig. 2.

The changes of surface hydrophobicity due to addition of TiO_2 nanoparticles and silane modification were evaluated in termsd of water contact angle measured using a goniometer. The surface is categorized as hydrophobic when the contact angle is more than 90°. The surface hydrophobicity is often affected by surface roughness and chemistry. The improvement of membrane hydrophobicity is important to reduce membrane wetting in membrane gas absorption. When the membrane is partially wetted or fully wetted by capillary condensation in the pores, the overall mass transfer coefficient will be reduced [29,32]. Fig. 3(a) shows that P0 membrane possesses a water contact angle of 121.1°. The alcohol bath induced roughness for the improvement of surface hydrophobicity similarly to the results obtained by Munirasu et al. [33]. Polymer crystallization and a liquid-liquid demixing were attributed to the roughness formation. After modification with silane, P0S membrane can achieve a water contact angle as high as 135.5° as shown in Fig. 3(b). Octadecyldimethylchlorosilane with a very low critical surface tension of 20-24 dynes/cm was expected to form hydrophobic surface on smooth substrate with a water angle more than 102°. As reported by [34], the surface hydrophobicity of PVDF membrane increased about 26%, reaching a water contact angle of 92° after blending in octadecyldimethochorosilane modified SiO_2 nanoparticles. In this work, PT and PTS membranes were fabricated using TiO_2 nanoparticles to alter the roughness of PVDF membranes for the creation of superhydrophobic surface. The surface roughness of neat PVDF membrane could be improved from 0.41 μm to 0.62 μm after blending TiO_2 nanoparticles into the membrane as discussed in our previous work [22]. The water contact angle of PT membrane was the lowest value recorded as shown in Fig. 3(c), only 102.6° after blending the hydrophilic TiO_2 nanoparticles. After modification with silane, PTS/2 membrane could achieve a higher water contact angle of 115.0° (Fig. 3(d)). The water contact angle of PVDF membrane could be further increased to 148.8° as proven in Fig. 3(e) when a higher concentration of silane was used to modify PTS/10 membrane. Hamzah [22] reported on a PVDF/TiO_2 membrane with water contact angle larger than 150° when fluoroalkylsilane was used to modify PVDF/TiO_2 membrane. However, the use of fluoroalkyl group with lower surface energy in the modification of membrane should not be encouraged as pre and polyfluoroalkyl substances (PFAs) have been linked to adverse health effects by the Environmental Protection Agency in the United States [35]. The ratio of fluoro-free silane used for modification should be further adjusted in the future work to improve the surface contact angle.

FT-IR spectra of P0, P0S, PT and PTS membranes in Fig. 4 show slight difference in chemical properties although they possess the same characteristic peaks of PVDF. PVDF characteristic peaks include the peaks at 2,850 cm^{-1} as well as 2,918 cm^{-1} resulted from the CH_2 asymmetric and symmetric vibration, respectively [36]. They also showed CH_2 wagging vibration at 1,401 cm^{-1} and C-C bonding at 1,165 cm^{-1}. The peak at 839 cm^{-1} is attributed to C-F stretching vibration, while the peak at 877 cm^{-1} is caused by C-C-C asymmetrical stretching vibration. After the addition of TiO_2 nanoparticles, the typical vibrations for Ti-O bonds ranging from 770 to 800 cm^{-1} were shown by PT and PTS membranes [37]. The slight difference was caused by the addition of TiO_2 via blending shown in green circle and the introduction of chemical groups via silane modification shown in blue circle at the range of 1,000-1,100 cm^{-1}

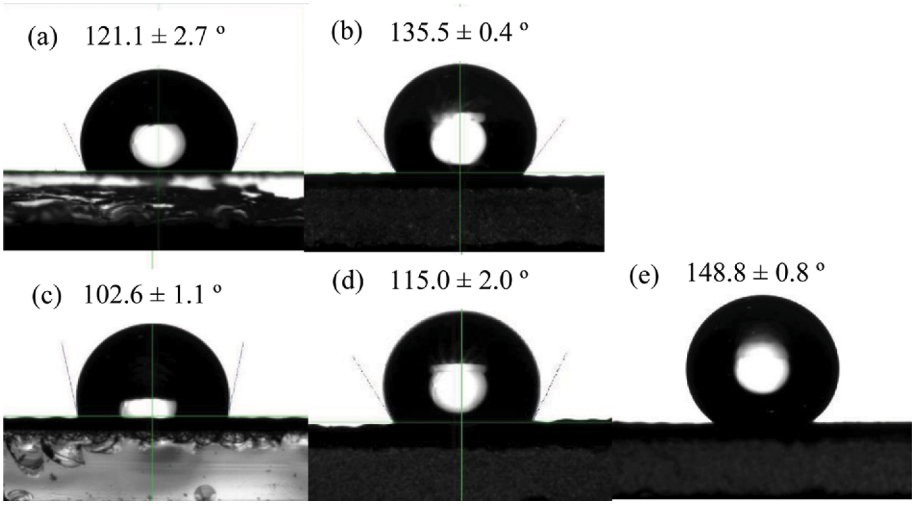

Fig. 3. WCA on (a) P0, (b) P0S, (c) PT and (d) PTS/2 and (e) PTS/10 membranes.

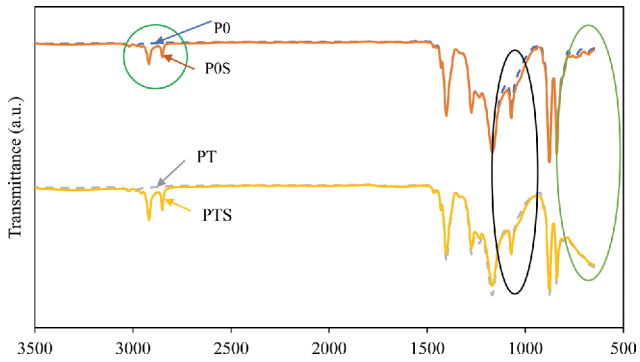

Fig. 4. FT-IR spectra of P0, P0S, PT and PTS/2 membranes.

due to the existence of Si-O-Si groups of silanes [38]. The absence of O-H stretching band at 3,500 cm^{-1} in FTIR spectra after silane modification indicated that the membranes are solvent-free after rising and drying.

2. Membrane Gas Absorption

CO_2 gas absorption with distilled water as the absorbent was conducted using a gas-liquid membrane contactor operated at room temperature and pressure. The liquid flow rate was set at 150 mL/min, while the gas flow rate was controlled at 100 mL/min. The absorption flux of CO_2 increased proportionally with the increasing flow rate of feed gas and absorbent because the higher flow rate resulted in higher mass transfer coefficient in gas or liquid phase as reported in our previous work [26]. The CO_2 absorption flux through different membranes is summarized in Table 2. Blending TiO_2 nanoparticles affected membrane pore size, porosity and wetting as discussed previously. Hence, the CO_2 absorption flux of PT membrane is slightly lower than P0 membrane. However, the reduction of surface energy with silane enhanced the CO_2 absorption significantly. The CO_2 absorption flux for P0S membrane is 79.2% higher than P0 membrane. From Table 2, the CO_2 absorption flux for PTS/10 membrane is the highest compared to P0, P0S, PT and PTS/2 membranes. A great improvement of CO_2 absorption flux by as much as 114% was achieved by using PTS/10 membrane in comparison to the neat PVDF membrane (P0). The improvement could be related to the improvement of membrane hydrophobicity as discussed earlier. The result obtained in this work was compared with recent works [25,26,39,40] as shown in Table 3. The absorption flux of PTS/10 membrane is comparable to those hollow fiber membranes and mixed matrix membranes with larger pore size but lower water contact angle.

Table 2. CO_2 absorption flux of fabricated membranes using distilled water as absorbent

Membrane	CO_2 absorption flux ($\times 10^{-4}$ mol·$m^{-2}s^{-1}$)
P0	2.88±0.17
P0S	5.16±0.26
PT	2.07±0.08
PTS/2	3.65±0.36
PTS/10	6.18±0.14

The prepared membranes were further tested using 0.01 M NaOH as the CO_2 absorbent in MGA system. Since the absorbed CO_2 forms carbonic acid in aqueous solution, NaOH is expected to react with carbonic acid. The remaining NaOH in the recycled absorbent stream was determined from the acid titration at varied interval time. The formation of carbonates and bicarbonates was calculated based on the remaining amount of NaOH after reacting with carbonic acid. The results obtained in Fig. 5 show that NaOH concentration decreased with time. More carbonates ions were expected to form over time, while bicarbonates ions would only appear when NaOH depleted completely. Similar observation was reported by Salmón et al. [17] who used polypropylene (PP) hollow fibers in MGA to facilitate CO_2 absorption into NaOH. However, the complete depletion of NaOH was only observed when P0S and PTS/10 membranes were treated with high concentration of silane solution used in membrane gas absorption. Although NaOH causes dehydrofluorination of PVDF membrane as reported by others [41,42], the silane modified membranes were less affected even using NaOH absorbent. The water contact angles of P0S and PTS/10 membranes dropped less than 8% after contact with NaOH absorbent for 200 min (supplementary document, Fig. S1). The improvement could be attributed to octadecyltrichloro silane layer on membrane surface which provides additional resistance towards dehydrofluorination [43]. More interestingly, P0S and PTS/10 membranes with different water contact angles showed similar carbonation potential. In 2D numerical simulation of membrane gas absorption using NaOH and amines, Nakhjiri et al. [44] highlighted

Table 3. Comparison the carbon capture performance of PTS/10 membrane to PVDF membranes reported in literature

Membrane	Form	CO_2 flow rate (ml/min)	Absorbent flow rate (ml/min)	Absorption flux (mol·m^{-2}·s^{-1})	References
PVDF	HF[a]	100	200	4.1×10^{-4}	[34]
PVDF/MMT[b]	HF[a]	150	50	9.7×10^{-4}	[35]
PVDF/20PBI	Flat	100	182	4.16×10^{-4}	[21]
PVDF/SAPO-34	Flat	100	204	6.67×10^{-4}	[22]
PTS/10	Flat	100	150	6.18×10^{-4}	This work

[a]Hollow fiber
[b]Montmorillonite
[c]Polybenzimidazole
[d]Silicoaluminophosphate

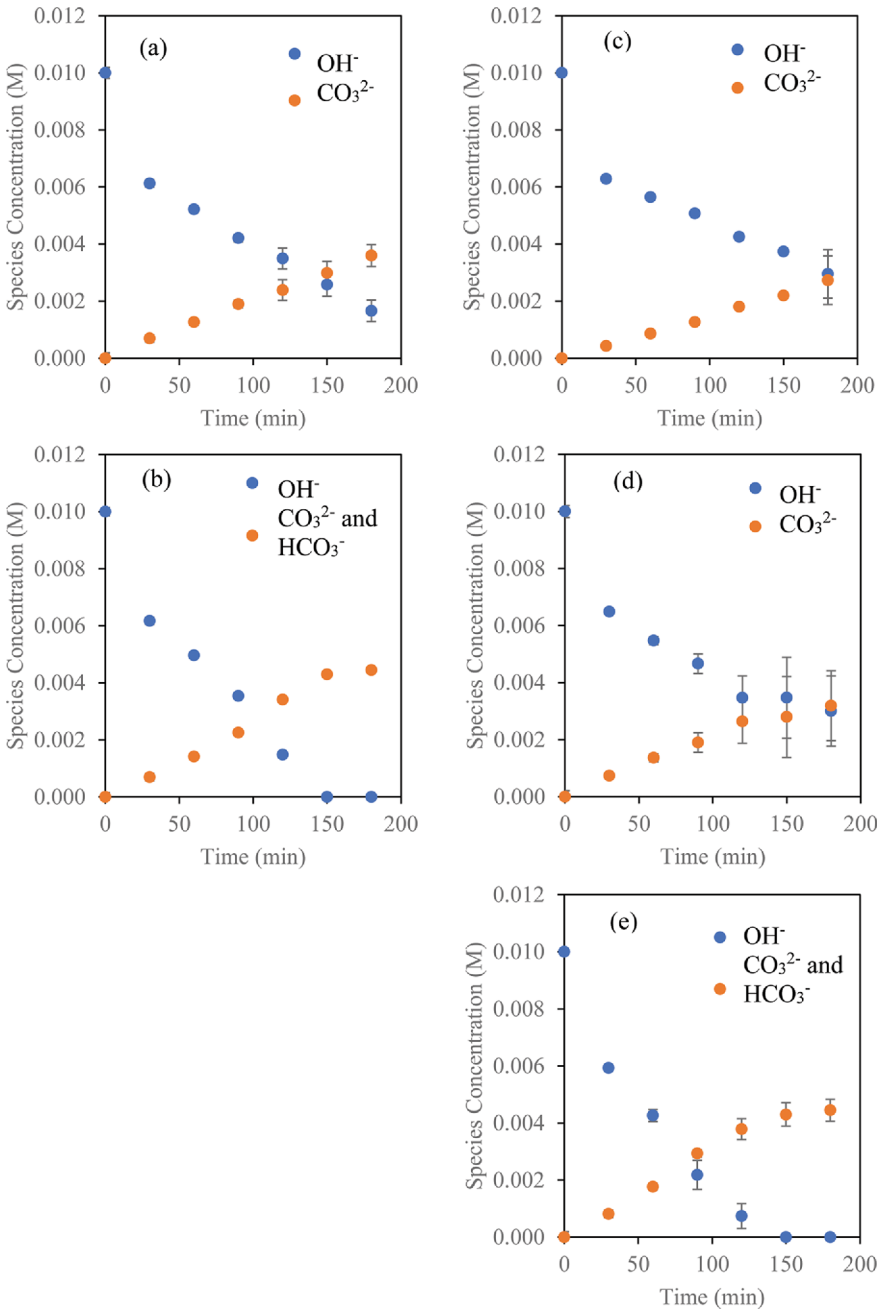

Fig. 5. Concentration of hydroxide, carbonate and bicarbonate versus time for (a) P0, (b) P0S, (c) PT (d) PTS/2 and (e) PTS/10 membrane.

that 40% of membrane wetting can cause up to 33% reduction of CO_2 permeation, but the non-wetted membranes can raise the CO_2 permeation more than four times. Although a high temperature is favorable in the irreversible reaction between CO_2 and NaOH, high temperature causes the absorbent vapor to fill the membrane pores and increase the total mass-transfer resistance [19]. More detailed study should be conducted to confirm if different mineral carbonation reactions will be affected by membrane wetting as well.

CONCLUSIONS

PVDF and PVDF/TiO_2 membranes with spongy porous structure were successfully fabricated. Membrane modification using octadecyltrichloro silane resulted in the growth of non-wetting layer on membrane surface. TiO_2 nanoparticles promoted the formation of this self-assembled monolayer by providing surface hydroxyl groups for the condensation of silanol groups after the hydrolysis of chlorosilane groups with alcohol. Hence, the water contact angle of PVDF/TiO_2 membrane could be increased to 148.8° using concentrated silane solution, nearly superhydrophobic. FT-IR spectra showed the difference of chemical properties of membranes after blending with TiO_2 nanoparticles and modification with octadecyltrichloro silane. The non-wetting surface helped to promote CO_2 absorption into water, as much as 114%. More importantly, the

silane modified membranes could be used for alkaline carbonation. The complete depletion of NaOH was achieved with the minimum changes of water contact angle observed. Further studies should be conducted on the carbonation of alkaline waste using the developed membrane for achieving simultaneous carbon capture and utilization.

ACKNOWLEDGEMENTS

The authors would like to acknowledge the financial support from Ministry of Education Malaysia (FRGS, 203.PJKIMIA.6071389) and Universiti Sains Malaysia (RUI 1001.PJKIMIA.8014060).

SUPPORTING INFORMATION

Additional information as noted in the text. This information is available via the Internet at http://www.springer.com/chemistry/journal/11814.

REFERENCES

1. International Energy Agency, https://www.iea.org/geco/.html, (accessed 16 August 2019).
2. Equinor, https://www.equinor.com/en/news/2019-06-12-sleipner-co2-storage-data.html, (accessed 16 August 2019).
3. NRG, https://www.nrg.com/case-studies/petra-nova.html, (accessed 16 August 2019).
4. B. A. Kader, https://gulfnews.com/business/energy/abu-dhabis-carbon-captureproject-on-track-1.1458076.html, (accessed 16 August 2019).
5. Y. Tanaka, Y. Sawada, D. Tanase, J. Tanaka, S. Shiomi and T. Kasukawa, *Energy Procedia*, **114**, 5836 (2017).
6. Department of Energy, https://www.energy.gov/fe/articles/doe-announces-major-milestone-reached-illinois-industrial-ccs-project, (accessed 16 August 2019).
7. A. Murnandari, J. Kang, M. H. Youn, K. T. Park, H. J. Kim, S.-P. Kang and S. K. Jeong, *Korean J. Chem. Eng.*, **34**, 935 (2017).
8. L. Ji and H. Yu, in *Carbon dioxide sequestration in cementitious construction materials*, F. Pacheco-Torgal, C. Shi and A. P. Sanchez Eds., Woodhead Publishing, London (2018).
9. D. Kang, S. Park, H. Jo and J. Park, *Chem. Eng. J.*, **248**, 200 (2014).
10. S. Park, J. Min, M.-G. Lee, H. Jo and J. Park, *Chem. Eng. J.*, **231**, 287 (2013).
11. S. Park, H. Jo, D. Kang and J. Park, *Energy*, **75**, 624 (2014).
12. Y. Zhao, J. Yuan, J. Zhang, L. Xie, Z. Ji, M. Su and J. Chen, *Desalination*, **322**, 151 (2013).
13. Y. Zhao, Y. Zhang, J. Liu, J. Gao, Z. Ji, X. Guo, J. Liu and J. Yuan, *Desalination*, **407**, 85 (2017).
14. W. Cheng, L. Fang, H. Cheng, E. Li, C. Zhang and F. Cheng, *J. Ind. Eng. Chem.*, **76**, 215 (2019).
15. A. Dindi, D. V. Quang, I. AlNashef and M. R. M. Abu-Zahra, *Desalination*, **442**, 62 (2018).
16. N. Zhang, R. M. Santos, S. M. Smith and L. Šiller, *Chem. Eng. J.*, **377**, 120479 (2019).
17. I. Salmón, N. Cambier and P. Luis, *Appl. Sci.*, **8**, 996 (2018).
18. L. Ji, H. Yu, B. Yu, K. Jiang, M. Grigore, X. Wang, S. Zhao and K. Li, *Chem. Eng. J.*, **352**, 151 (2018).
19. J.-L. Li and B.-H. Chen, *Sep. Purif. Technol.*, **41**, 109 (2005).
20. M. F. Rabuni, N. M. Nik Sulaiman, M. K. Aroua and N. A. Hashim, *Ind. Eng. Chem. Res.*, **52**, 15874 (2013).
21. A. T. Nakhjiri, A. Heydarinasab, O. Bakhtiari and T. Mohammadi, *Chin. J. Chem. Eng.*, **26**, 1845 (2018).
22. N. Hamzah, C. P. Leo and B. S. Ooi, *Chin. J. Polym. Sci.*, **37**, 609 (2019).
23. A. Rosli, A. L. Ahmad and S. C. Low, *Sep. Purif. Technol.*, **221**, 275 (2019).
24. N. Hamzah and C. P. Leo, *Sep. Purif. Technol.*, **167**, 79 (2016).
25. N. A. Ahmad, C. P. Leo, A. L. Ahmad and A. W. Mohammad, *Int. J. Hydrogen Energy*, **41**, 4855 (2016).
26. N. A. Ahmad, A. N. Mohd Noh, C. P. Leo and A. L. Ahmad, *Chem. Eng. Res. Des.*, **118**, 238 (2017).
27. M. Tomaszewska, *Desalination*, **104**, 1 (1996).
28. S. H. Elahi and I. C. Escobar, in *Modern applications in membrane science and technology*, I. Escobar and B. V. der Bruggen Eds., American Chemical Society, Washington (2011).
29. A. L. Ahmad, A. R. Sunarti, K. T. Lee and W. J. N. Fernando, *Int. J. Greenh. Gas Con.*, **4**, 495 (2010).
30. C. P. Tripp and M. L. Hair, *Langmuir*, **8**, 1120 (1992).
31. O. Benhabiles, F. Galiano, T. Marino, H. Mahmoudi, H. Lounici and A. Figoli, *Molecules*, **24**, 724 (2019).
32. S.-W. Park, D.-S. Suh, K.-S. Hwang and H. Kumazawa, *Korean J. Chem. Eng.*, **14**, 285 (1997).
33. S. Munirasu, F. Banat, A. A. Durrani and M. A. Haija, *Desalination*, **417**, 77 (2017).
34. R. J. Mistry, M. Saxena, P. Ray and P. S. Singh, *J. Appl. Polym. Sci.*, **135**, 46043 (2018).
35. Agency for Toxic Substances and Disease Registry, https://www.health.pa.gov/topics/Documents/Environmental%20Health/PFAS%20Exposure%20Assessment%20Technical%20Tools.pdf.html, (accessed 16 August 2019).
36. H. Bai, X. Wang, Y. Zhou and L. Zhang, *Pro. Nat. Sci. Mater.*, **22**, 250 (2012).
37. G. C. Collazzo, S. L. Jahn, N. Carreño and E. L. Foletto, *Braz. J. Chem. Eng.*, **28**, 265 (2011).
38. J. Coates, in *Encyclopedia of analytical chemistry*, R. A. Meyers Ed., John Wiley & Sons, Chichester (2006).
39. A. Mansourizadeh and A. F. Ismail, *Int. J. Greenh. Gas Con.*, **5**, 374 (2011).
40. M. Rezaei, A. F. Ismail, S. A. Hashemifard, G. Bakeri and T. Matsuura, *Int. J. Greenh. Gas Con.*, **26**, 147 (2014).
41. N. Awanis Hashim, Y. Liu and K. Li, *Chem. Eng. Sci.*, **66**, 1565 (2011).
42. Q. Wu, X. Zhang and G. Cao, *J. Environ. Sci.*, **67**, 294 (2018).
43. J. Li, L. Yan, H. Li, J. Li, F. Zha and Z. Lei, *RSC Adv.*, **5**, 53802 (2015).
44. A. T. Nakhjiri, A. Heydarinasab, O. Bakhtiari and T. Mohammadi, *J. Environ. Chem. Eng.*, **6**, 1500 (2018).